

Infrared Imaging of $z = 2.43$ Radio Galaxy B3 0731+438 with the Subaru Telescope — Detection of H α Ionization Cones of a Powerful Radio Galaxy

Kentaro MOTOHARA, Fumihide IWAMURO, Hiroshi TERADA, Miwa GOTO,
Jun'ichi IWAI, Hirohisa TANABE, Tomoyuki TAGUCHI, Ryuji HATA,
Toshinori MAIHARA,

Department of Physics, Kyoto University, Kitashirakawa, Kyoto 606-8502
E-mail(KM): motohara@cr.scphys.kyoto-u.ac.jp

Shin OYA,

Communications Research Laboratory, Koganei, Tokyo 184-8975

Masanori IYE,

Optical and Infrared Astronomy Division, National Astronomical Observatory, Mitaka, Tokyo 181-8588

George KOSUGI, Jun'ichi NOUMARU,

Ryusuke OGASAWARA, Toshinori SASAKI, and Tadafumi TAKATA

Subaru Telescope, National Astronomical Observatory, 650 North Aohoku Place, Hilo, HI 96720, USA

(Received 1999 October 28; accepted 1999 December 21)

Abstract

We report on infrared imaging observations of the $z = 2.429$ radio galaxy B3 0731+438 with the Subaru telescope. The images were taken with the K' -band filter and the $2.25 \mu\text{m}$ narrow-band filter to examine the structure and properties of the H α + [N II] $\lambda\lambda$ 6548, 6583 emission-line components. The H α + [N II] emission-line image shows biconical lobes with an extent of 40 kpc, which are aligned with the radio axis. The rest-frame equivalent widths of the emission lines at these cones are as large as 1100 Å, and can be well explained by a gas-cloud model photoionized by power-law continuum radiation. The isotropic ionizing photon luminosity necessary to ionize the hydrogen gas in these cones amounts to 10^{57} (photons s^{-1}), which is larger than that in the majority of radio-loud QSOs. From these results, we propose that the H α alignment effect in this object is produced by biconical gas clouds, which are swept up by the passage of radio jets, and are ionized by strong UV radiation from a hidden AGN. The continuum image consists of two components, a stellar-like point source and an extended diffuse galaxy. These are supposed to be a type-2 AGN and its host galaxy. The SED is fitted by a combination of spectra of a reddened dust-scattered AGN and an instantaneous starburst population of 500 Myr old. The stellar mass of the galaxy is estimated to be $3 \times 10^{11} M_{\odot}$, which is as large as that of typical 3C radio galaxies at $z = 1$.

Key words: AGN: ionization cone — galaxies: active — galaxies: individual (B3 0731+438) — infrared: galaxies

1. Introduction

It is well known that in high-redshift radio galaxies, the elongated morphologies of the emission lines and rest-frame UV continuum light are often aligned with the radio axes (McCarthy et al. 1987; Chambers et al. 1987). The cause of this “alignment-effect” is still unclear, although it is almost certain that this phenomenon is due to the anisotropic structures of AGNs at the centers of the galaxies. Several hypotheses have been suggested, such as induced star formation by the passage of radio jets (Rees 1989; Begelman, Cioffi 1989; de Young 1989), inverse-Compton scattering of cosmic-background radiation (Daly 1992a, 1992b), dust or electron scattering

of anisotropic radiation from a hidden AGN (di Serego Alighieri et al. 1989; Fabian 1989), and nebular emission from surrounding clouds ionized by UV radiation from a central engine (Dickson et al. 1995).

To examine the structure and properties of the H α emission-line region in a high-redshift radio galaxy, we carried out high-resolution infrared imaging observations of a powerful radio galaxy, B3 0731+438, at $z = 2.429$ in the K' -band and the $2.25 \mu\text{m}$ narrow-band. This object is a typical FR II radio galaxy with strong double-lobed radio-emitting hot spots and a central core (Carilli et al. 1997). The optical R -band image shows a diffuse morphology with a few knots, while the narrow-band image

presents aligned Ly α emission clouds (McCarthy 1991). The optical spectrum displays an extremely strong Ly α emission line with a rest-frame equivalent width of 900 Å (McCarthy 1991), which is one of the the largest values among known high- z radio galaxies. Infrared spectra reveal a strong H α + [N II] emission line (McCarthy et al. 1992; Eales, Rawlings 1993; Evans 1998), contributing 20 – 30% flux in the K -band. Diagnostic emission-line ratios are consistent with the presence of a Seyfert 2 nucleus (Evans 1998).

We describe our observations and data reductions in section 2, and present the results in section 3. Discussions are presented in section 4 and we summarize them in section 5. Cosmological constants are assumed to be $H_0 = 50 \text{ km s}^{-1} \text{ Mpc}^{-1}$ and $q_0 = 0.1$ throughout this paper. The scale at $z = 2.429$ is thus $11.3 \text{ kpc}''$, and the look-back time is 13 Gyr, while the age of the universe is 16.5 Gyr.

2. Observations and Data Reduction

2.1. Observations

B3 0731+438 was observed using a $2.25 \mu\text{m}$ narrow-band filter ($\lambda/\Delta\lambda = 100$) on 1999 February 25 and 27, and using a K' -band filter on February 27, with a near-infrared camera CISCO (Motohara et al. 1998) mounted on the Cassegrain focus of the Subaru telescope. The total field of view of the camera was $\sim 2' \times 2'$ with a pixel scale of $0''.116 \text{ pixel}^{-1}$. The exposure time of a single frame was 60 s for the narrow-band and 20 s for the K' -band images. To subtract the background sky emission, we nodded the telescope slightly ($\sim 10''$) and acquired 6 (narrow-band) or 12 (K' -band) frames at each of eight different positions, resulting in 48 or 96 frames per each dataset, respectively. The total exposure time was 5760 s for the narrow-band and 1920 s for the K' -band. The atmospheric conditions were photometric and the seeing was stable during the observation, which was $0''.6$ on February 25 and $0''.4$ on 27. The logs of the observations are summarized in table 1.

2.2. Data Reduction

We carried out data reduction of the K' -band frames as follows. First, a “standard K' flat” frame was produced by median-averaging 250 available K' -band frames taken on February 23, 25, and 27, excluding the B3 0731+438 frames. Then, every B3 0731+438 frame was divided by the standard K' flat frame. After applying cosmetic corrections for bad pixels, we made a “sky” frame by median-averaging the frames of which prominent objects were masked and replaced by the surrounding sky value with appropriate noise. We smoothed this sky frame with a 20×20 pixels boxcar filter, normalized the average of

the pixel value to unity and multiplied it by the standard K' flat frame to make a “self-calibrated K' flat” frame.

Using this self-calibrated K' flat frame, a sky frame was generated again by following the above procedure from the beginning, and was subtracted from each frame. The 12 frames in each set were shifted by a sub-pixel offset according to a reference star in the frames and averaged to create a “minor” frame. The final K' -band image was produced by median-averaging these minor frames. The seeing size of the final image was $0''.4$.

Narrow-band frames were processed in the same way as for the K' -band, except that no self-calibrated flat frame was produced, due to the small sky background flux in this band. Two versions of final narrow-band images were made: one was a “total” image produced from all the frames; the other was a “good-seeing” image produced only from the frames taken on February 27. The seeing size was $0''.6$ for the total image and $0''.4$ for the good-seeing image. We created a color image of B3 0731+438 from the K' -band and the “good-seeing” narrow-band image, which is shown in figure 1.

To investigate the emission-line and continuum properties of B3 0731+438, we made two post-processed images. One was a line-free continuum image (K -continuum image) produced by subtracting the scaled narrow-band image from the K' -band image. The other was a continuum-subtracted emission-line image (H α + [N II] image) produced by subtracting the scaled K -continuum image from the total narrow-band image. We present these images in figure 2 together with their contours.

3. Results

3.1. Photometry

The results of aperture photometry of B3 0731+438 are given in table 2 together with that of other observations. The aperture is $9''.4$ diameter. The flux calibration was done using images of UKIRT faint standard stars (FS 15, FS 21, and FS 23) taken before or after the observations. The K' - and narrow-band flux of the standard stars were calculated by interpolating their K - and H -band flux.

3.2. The K -Continuum Image

The K -continuum image of B3 0731+438 in figure 2b appears to comprise a very compact core and an extended diffuse nebula, which can be seen in the deconvolved image (figure 2c) more clearly. The compact core couldn't be resolved even with a spatial resolution as high as $0''.4$. Therefore, we modeled the K -continuum image with a two-component profile consisting of a stellar core and an exponential disk.

The profile of the core is assumed to be that of a field star fitted by a modified moffat function. The moffat

function is written as

$$I(x, y) = I_c \left[1 + \left(\frac{r}{\alpha} \right)^{-\beta} \right], \quad (1)$$

where r is the radial distance from the center. However, the stellar image is distorted elliptically because of imperfect operation of the telescope (mirror support, auto-guiding and so on) during the observations. We therefore had to introduce a PSF modification, defined as $r^2 = X^2 + Y^2$ and

$$\begin{pmatrix} X \\ Y \end{pmatrix} = \begin{pmatrix} \sqrt{1+e} & 0 \\ 0 & \sqrt{1-e} \end{pmatrix} \begin{pmatrix} \cos \Theta & -\sin \Theta \\ \sin \Theta & \cos \Theta \end{pmatrix} \begin{pmatrix} x \\ y \end{pmatrix}, \quad (2)$$

where Θ and e are the position angle and the ellipticity of a stellar image, respectively. The values of these parameters for the field stars are $\alpha = 0''.42$, $\beta = 3.1$, $\Theta = 45^\circ$, and $e = 0.12$.

We set five free parameters to reconstruct the K -continuum profile of B3 0731+438. They are the peak height, the position relative to the core profile, and the effective radius of the exponential disk and the peak height of the core. The results of the fitting are shown in figure 3, and the obtained photometric data are listed in table 2. The FWHM of the exponential disk profile is $1''.6$, which corresponds to 18 kpc. The peak of the disk is located at $0''.24$ south of the core.

3.3. The Emission-Line Image

The $\text{H}\alpha + [\text{N II}]$ image in figure 2a shows a unique morphology. Diffuse line emission extends out to $3''.3$ from the center, corresponding to 37 kpc. They are aligned with the axis of the radio hot spots, and both ends of the clouds fork into two directions. Such a morphology suggests the existence of biconical clouds radiating $\text{H}\alpha + [\text{N II}]$ emission lines. The total flux of $\text{H}\alpha + [\text{N II}]$ emission is $3.5 \times 10^{-18} \text{ W m}^{-2}$, which corresponds to a luminosity of $3.2 \times 10^{37} \text{ W}$.

We used square aperture photometry of the northern cone, the southern cone and the central core, which are marked as square boxes in figure 2. The results are listed in table 3. The most striking result is the extremely large rest-frame equivalent width of more than 1000 Å of the $\text{H}\alpha + [\text{N II}]$ line in the northern and southern cones. When the results of both cones are combined, the equivalent width at the cones is $1098_{-288}^{+516} \text{ Å}$.

4. Discussion

Few narrow-band imagings aimed at the rest-frame optical emission-line of powerful radio galaxies at a redshift of $z > 2$ have been carried out, because the lines redshift into the infrared wavelength. Armus et al. (1998) imaged the $[\text{O III}]$ emission-line morphology of $z = 3.594$ radio galaxy 4C 19.71 through a $2.3 \mu\text{m}$ narrow-band filter. They found a large ($\sim 70 \text{ kpc}$) aligned nebular,

whose length is the same as that of the separation of the radio hot spots. However, its morphology is like a ‘‘corridor’’ between the core and the radio hot spots, and does not show a conic structure. The total $[\text{O III}]$ luminosity is $2 \times 10^{37} \text{ W}$, which is comparable to a $\text{H}\alpha + [\text{N II}]$ luminosity of $3 \times 10^{37} \text{ W}$ of B3 0731+438, if we assume $[\text{O III}]/\text{H}\alpha + [\text{N II}] = 1$. Egami et al. (1999) observed the $\text{H}\alpha + [\text{N II}]$ emission-line morphology of $z = 2.269$ 4C 40.36, and found aligned $\text{H}\alpha + [\text{N II}]$ knots extended linearly over $\sim 20 \text{ kpc}$, but no emission-line cone was seen. They also found an unresolved ($< 2 \text{ kpc}$) continuum core, which we found in B3 0731+438.

4.1. Properties of Extended Emission Line Clouds

Concerning the emission mechanism of the aligned $\text{H}\alpha + [\text{N II}]$ morphology of B3 0731+438, there are four major hypotheses, as described before. Among them, it is impossible to explain the observed emission-line spectrum by the inverse-Compton scattering of the cosmic-background radiation, from which no spectrum feature is expected.

Regarding the second possibility of induced star formation, it is known that the Wolf-Rayet galaxy NGC 4861 shows a $\text{H}\alpha + [\text{N II}]$ equivalent width larger than 900 Å (McQuade et al. 1995). Model spectra of a few-Myr old galaxies also show equivalent widths larger than 1000 Å (Calzetti 1997). On the other hand, the shape of the $\text{L}\alpha$ cloud with an equivalent width of 900 Å reported by McCarthy (1991), is pinched at the peak of the K -continuum image, and matches the $\text{H}\alpha + [\text{N II}]$ morphology that we have observed. Such a morphology suggests that $\text{L}\alpha$ photons are radiated from the same region of the $\text{H}\alpha + [\text{N II}]$ cones, and that both emission lines have a common ionization source. Since a stellar system cannot account for an equivalent width of $\text{L}\alpha$ as large as 900 Å (Charlot, Fall 1993), we infer that the alignment of the $\text{H}\alpha + [\text{N II}]$ image is not caused by a star-forming region.

We cannot rule out the third possibility of scattered light of anisotropic radiation from the central engine by dust or electrons, because the maximum $\text{H}\alpha + [\text{N II}]$ equivalent widths of high-redshift QSOs observed are 800 Å (Baker et al. 1999; Hill et al. 1993; Espey et al. 1989) and our 1σ lower limit is 800 Å. We therefore evaluated the $\text{L}\alpha/\text{H}\alpha$ ratio to examine the contribution of nebular emission to the $\text{H}\alpha$ flux, because the extended $\text{L}\alpha$ emission is radiated as nebular emission. The observed $\text{L}\alpha/\text{H}\alpha$ is 5.5, assuming that all of the $\text{L}\alpha$ flux ($3.1 \times 10^{-18} \text{ W m}^{-2}$; McCarthy 1991) is radiated from the cones and that $\text{H}\alpha/[\text{N II}]=4$. On the other hand, $\text{L}\alpha/\text{H}\alpha$ under the case-B condition of the low-density limit is 8.75 (Binette et al. 1992), and only a small amount of dust, such as $E(B-V) = 0.04$, halves the ratio. We infer from this result that the majority of $\text{H}\alpha$ luminosity is not scattered light from the central engine, but nebular emission

radiated from the cones, itself.

Accordingly, we examined whether a gas cloud ionized by anisotropic UV radiation from a hidden AGN can reproduce an equivalent width as large as 1100 Å. First, we extracted the physical properties of the cones and the ionizing source from the data in table 3, using the same method as that carried out by Baum and Heckman (1989). Assuming the gas to be fully ionized and in the case-B condition, the luminosity of the H α emission line is written as

$$L(\text{H}\alpha) = n_e^2 \alpha_{\text{H}\alpha}^{\text{eff}} h \nu_{\text{H}\alpha} V f, \quad (3)$$

where n_e is the electron density, h the Planck constant, $\nu_{\text{H}\alpha}$ the frequency of the H α line, V the volume of the line emitting region, f the volume filling factor, and $\alpha_{\text{H}\alpha}^{\text{eff}} = 6.04 \times 10^{-14} \text{ (cm}^3 \text{ s}^{-1}\text{)}$ (Osterbrock 1989), the H α recombination coefficient under case-B. We assumed $\text{H}\alpha/[\text{N II}] = 4$ according to simulations by CLOUDY90 (see following) and took V for a cylinder and a half-cut cylinder for the northern and southern cones, respectively.

Because we do not know the volume filling factor, f , we must estimate it from direct measurements of other radio galaxies. From measurements of the density of ionized gas using sulphur lines in low-redshift radio galaxies, their filling factor is estimated to be in range $10^{-4} - 10^{-5}$ (Heckman et al. 1982; van Breugel et al. 1985). While the same value is observed in a high-redshift radio galaxy (Rush et al. 1997), we adopted the value $f = 10^{-4}$. However, the reader should keep in mind that this value is uncertain and may differ by an order of magnitude.

The mass of the line emission gas was calculated using the relation

$$M_{\text{gas}} = V f n_e m_{\text{H}}, \quad (4)$$

where m_{H} is the hydrogen mass. We next assumed that the line emission gas was filling the cones at the beginning, and was swept up by the passage of radio jets. We thus deduced the total mass of the gas surrounding the galaxy $M_{\text{tot}} = M_{\text{gas}} \frac{4\pi}{\Omega}$, taking the opening angles of the cones Ω to be 0.12π str and 0.06π str for the northern and southern cones, respectively.

The number of ionizing photons Q can be written as (Osterbrock 1989)

$$Q = \frac{\alpha_{\text{B}}}{\alpha_{\text{H}\alpha}^{\text{eff}}} \frac{L(\text{H}\alpha)}{h \nu_{\text{H}\alpha}}, \quad (5)$$

where $\alpha_{\text{B}} = 1.43 \times 10^{-13}$ is the total recombination coefficient under the case-B condition. The total number of ionizing photons radiated by the central engine was calculated as $Q_{\text{tot}} = Q \frac{4\pi}{\Omega f_c}$, where f_c is the covering factor of the cloud in the cone.

At last, the ionization parameter of the clouds is defined as

$$U = \frac{Q}{R^2 \Omega f_c n_e c}, \quad (6)$$

where R is the distance of the cloud from the central engine and c the velocity of light. Because we do not know the covering factor, f_c , we calculated the lower limits of Q_{tot} and U assuming $f_c = 1$.

All of these calculated values are given in table 4. The electron density is on the order of 50 (cm^{-3}), the ionization parameter 0.001, and the mass of the emission line cloud $10^9 M_{\odot}$. These values are similar to those deduced for the ~ 100 kpc extended line emission clouds of other high-redshift radio galaxies (Rush et al. 1997; Heckman et al. 1991). The large luminosity of the ionizing photons ($> 10^{57}$ photons s^{-1}) draws our attention, which is far larger than the values for typical low- z radio galaxies (10^{51-54} photons s^{-1}) (Baum, Heckman 1989), even larger than that of radio loud QSOs (10^{54-56} photons s^{-1}) (Stockton, MacKenty 1987), and almost comparable to that of the brightest QSOs (10^{57-58} photons s^{-1}) (Hill et al. 1993). Here, we calculated the luminosity of ionizing photons for QSOs from their $L(\text{H}\alpha)$ using equation (5), or from $L(\text{H}\beta)$ with $L(\text{H}\alpha)/L(\text{H}\beta) = 4$ taken from Kwan and Krolik (1981).

Next, we carried out a photoionization calculation using the code CLOUDY90 (Ferland et al. 1998) by assuming a wide range of hydrogen density, n_{H} , and ionization parameter, U . The cloud distance from an ionizing source was set to 25 kpc and its thickness to 100 pc. We assumed the metal abundance to be $Z = 0.1 Z_{\odot}$, according to the observations of $z \sim 2$ damped Ly α clouds (Pettini et al. 1994). The continuum spectrum of the ionizing source is set to a power law, $f_{\nu} \propto \nu^{\alpha}$, with $\alpha = -0.7$ longward of 912 Å and $\alpha = -2.5$ shortward of 912 Å, taken from the composite spectrum of radio-loud QSOs (Cristiani, Rio 1990; Zheng et al. 1997). The resultant equivalent widths, calculated from the emission-line strength and the diffuse continuum radiation, are shown in table 5. Most of the simulated equivalent widths exceed 1000 Å, satisfying the observed value.

Thus, we suggest that the emission mechanism of the extended H α + [N II] cones of B3 0731+438 is nebular emission from clouds ionized by the strong UV radiation of the hidden AGN.

4.2. Spectral Energy Distribution

Assuming that the exponential disk component of the K -continuum image is a host galaxy of B3 0731+438 and the compact core a type-2 AGN, we reconstructed the SED of the B3 0731+438 with model spectra of a type-2 AGN and a galaxy. Because contamination of the [O II] $\lambda\lambda$ 3727 emission line to the J -band flux is expected,

we subtracted it, assuming an $H\alpha/[O\ II]$ ratio of 3 (McCarthy et al. 1995). The model spectrum of the galaxy was calculated by the spectrophotometric galaxy evolution model PEGASE (Fioc, Rocca-Volmerange 1997) under three variations of star-forming history, namely, an instantaneous burst model, and two exponential burst models with time scales of $\tau = 200$ Myr and 2 Gyr, respectively. For the model spectrum of the type-2 AGN, we selected the dust-scattered AGN model calculated by Cimatti et al. (1994) with a scattering angle, Θ , of 90° and the power-law index of the incident continuum being $\alpha = -0.7$, and assuming extinction of SMC dust (Prévot et al. 1984, Bouchet et al. 1985). We scaled these two spectra according to their observed K -continuum flux and fit the J - and R -band flux by altering the age of the galaxy and the extinction of the type-2 AGN.

We show the results in figure 4 and table 6. The $\tau = 2$ Gyr exponential burst model is not plausible, because the age of the best-fit galaxy model is 10 Gyr, which is larger than the cosmic age (3.5 Gyr for the assumed cosmological parameters). Both the $\tau = 200$ Myr exponential burst model and the instantaneous burst model fit the SED. However, we prefer the instantaneous burst model because the observed flux of the R -band appears to be dominated by the diffuse galactic component, as can be seen in the R -band image of McCarthy (1991).

Consequently, we suppose that the age of the galaxy is 500 Myr, resulting in a formation redshift of $z_{\text{form}} \sim 3$. The total stellar mass of the galaxy estimated from the model is $3 \times 10^{11} M_\odot$, comparable to that of a typical 3C radio galaxy at $z = 1$ (Best et al. 1997).

The $H\alpha+[N\ II]$ peak is located at the center of the galaxy and aligned to the radio axis. Infrared spectroscopic observations showed that the $H\alpha$ line width is narrow ($< 560\text{ km s}^{-1}$; McCarthy et al. 1992) and that the emission-line ratios are similar to those of Seyfert 2 galaxies (Evans 1997). We therefore suggest that the $H\alpha+[N\ II]$ luminosity at the center of the galaxy is dominated by scattered radiation from the narrow-line regions of the hidden nucleus. However, the possibility of intense starburst activity cannot be ruled out entirely, and polarimetry is necessary for a confirmation.

5. Summary and Conclusions

We observed the powerful radio galaxy B3 0731+438 in the infrared K' -band and the $2.25\ \mu\text{m}$ narrow-band, corresponding to the rest-frame 6000 Å continuum and $H\alpha+[N\ II]$ emission line, respectively. We then produced a line-free K -continuum image and a continuum-subtracted $H\alpha+[N\ II]$ emission-line image.

Our observations are the first to show a cone-shaped $H\alpha+[N\ II]$ emission-line structure of a high-redshift radio galaxy at infrared wavelength. The radio-aligned cones suggest that the gas is ionized by the hidden AGN. The

contribution of the scattered light from the hidden AGN to the $H\alpha$ luminosity is estimated to be small. On the other hand, we find that a gas cloud ionized by a power-law UV continuum can account for the large observed $H\alpha+[N\ II]$ equivalent width, using the values of the electron density and the ionization parameter estimated from the observed $H\alpha$ line luminosity. Together with their biconical structure, we infer that we have detected $H\alpha$ ionization cones of a high-redshift powerful radio galaxy for the first time. The estimated mass of the ionized gas cones is of the order of $10^9 M_\odot$, and the expected total mass of the gas surrounding the galaxy is $10^{11} M_\odot$.

The $H\alpha+[N\ II]$ peak at the center of the galaxy is also aligned to the radio axis. We suppose that this peak is scattered light from the narrow-line regions of the hidden AGN, and that polarimetry is necessary for a confirmation.

The K -continuum image is separated into two components, assumed to be a type-2 AGN and an underlying host galaxy. The SED of the whole radio galaxy is modeled by a model spectrum of a 500 Myr-old instantaneous burst galaxy and dust-scattered power-law continuum with $A_V = 1.9$ mag extinction. The stellar mass of the galaxy is $3 \times 10^{11} M_\odot$, which is comparable to that of a typical 3C radio galaxy at $z = 1$.

We thank all staff of the Subaru Telescope, who supported us to set up our instrument, and helped us to make these observations. We would like to express our thanks to the engineering staff of Mitsubishi Electric Co. for their fine operation of the telescope during the test observation runs, and the staff of Fujitsu Co. for timely provision of control software.

We also appreciate M. Fioc and B. Rocca-Volmerange for generously offering their galaxy modeling code, PEGASE, and G. Ferland for the spectral synthesis code, CLOUDY90.

K.Motohara was financially supported by the Japan Society for the Promotion of Science.

References

- Armus L., Soifer B.T., Murphy T.W.Jr, Neugebauer G., Evans A.S., Matthews K. 1998, ApJ 495, 276
- Baker J.C., Hunstead R.W., Kapahi V.K., Subrahmanya C.R. 1999, ApJS 122, 29
- Baum S.A., Heckman T. 1989, ApJ 336, 681
- Begelman M.C., Cioffi D.F. 1989, ApJ 345, L21
- Best P.N., Longair M.S., Röttgering H.J.A. 1997, MNRAS 292, 758
- Binette L., Magris G., Bruzual G. 1992, in Relationship Between Active Galactic Nuclei and Starburst Galaxies, ed A. V. Filippenko, ASP Conf. Ser. 31, 211
- Bouchet P., Lequeux J., Maurice E., Prévot L., Prévot-Burnichon M.L. 1985, A&A 149, 330
- Calzetti D. 1997, AJ 113, 162
- Carilli C.L., Röttgering H.J.A., van Ojik R., Miley G.K., van Breugel W.J.M. 1997, ApJS 109, 1
- Chambers K., Miley G., van Breugel W. 1987, Nature 329, 604
- Charlot S., Fall S.M. 1993 ApJ 415, 580
- Cimatti A., di Serego Alighieri S., Field G.B., Fosbury R.A.E. 1994, ApJ 422, 562
- Cristiani S., Vio R. 1990, A&A 227, 385
- Daly R.A. 1992a, ApJ 386, L9
- Daly R.A. 1992b, ApJ 399, 426
- de Young D.S. 1989, ApJ 342, L59
- Dickson R., Tadhunter C., Shaw M., Clark N., Morganti R. 1995, MNRAS 273, L29
- di Serego Alighieri S., Fosbury R.A.E., Quinn P.J., Tadhunter C.N. 1989, Nature 341, 307
- Eales S.A., Rawlings S. 1993, ApJ 411, 67
- Egami E., Armus L., Neugebauer G., Soifer B.T., Evans A.S., Murphy T.W.Jr 1999, in The Hy-Redshift Universe: Galaxy Formation and Evolution at High Redshift, ed A.J. Bunker and W.J.M. van Breugel, ASP Conf. Ser. in press (astro-ph/9909517)
- Espey B.R., Carswell R.F., Bailey J.A., Smith M.G., Ward M.J. 1989, ApJ 342, 666
- Evans A.S. 1998, ApJ 498, 553
- Fabian A.C. 1989, MNRAS 238, 41p
- Ferland G.J., Korista K.T., Verner D.A., Ferguson J.W., Kingdon J.B., Verner E.M. 1998, PASP 110, 761
- Fioc M., Rocca-Volmerange B. 1997, A&A 326, 950
- Heckman T.M., Lehnert M.D., Miley G.K., van Breugel W. 1991, ApJ 381, 373
- Heckman T.M., Miley G.K., Balick B., van Breugel W.J.M., Butcher H.R. 1982, ApJ 262, 529
- Hill G.J., Thompson K.L., Elston R. 1993, ApJ 414, L1
- Kwan J., Krolik J.H. 1981, ApJ 250, L478
- McCarthy P.J. 1991 AJ 102, 518
- McCarthy P.J., Elston R., Eisenhardt P. 1992, ApJ 387, L29
- McCarthy P.J., Spinrad H., van Breugel W. 1995 ApJS 99, 27
- McCarthy P.J., van Breugel W., Spinrad H., Djorgovski S. 1987, ApJ 321, L29
- McQuade K., Calzetti D., Kinney A.L. 1995, ApJ 97, 331
- Motohara K., Maihara T., Iwamuro F., Oya S., Imanishi M., Terada H., Goto M., Iwai J. et al. 1998, Proc. SPIE 3354, 659
- Osterbrock D.E. 1989, Astrophysics of Gaseous Nebulae and Active Galactic Nuclei (University Science Books, Mill Valley)
- Pettini M., Smith L.J., Hunstead R.W., King D.L. 1994, ApJ 426, 79
- Prévot M.L., Lequeux J., Maurice E., Prévot L., Rocca-Volmerange B. 1984, A&A 132, 389
- Rees M.J. 1989, MNRAS 239, 1p
- Rush B., McCarthy P.J., Athreya R.M., Persson S.E. 1997, ApJ 484, 163
- Stockton A., MacKenty J.W. 1987, ApJ 316, 584
- van Breugel W., Miley G., Heckman T., Butcher H., Bridle A. 1985, ApJ 290, 496
- Zheng W., Kriss G.A., Telfer R.C., Grimes J.P., Davidsen A.F. 1997, ApJ 475, 469

Table 1. Observational logs of B3 0731+438.

Date	Object	Band	Exposure	Seeing
1999 February 25	B3 0731+438	N225	60 s \times 48	0''6
	FS 21	N225	10 s \times 24	
1999 February 27	FS 15	K'	2 s \times 24	0''4
	FS 15	N225	10 s \times 24	
	B3 0731+438	K'	20 s \times 96	
	B3 0731+438	N225	60 s \times 48	
	FS 23	K'	10 s \times 24	

Table 2. Photometric data of B3 0731+438.

Band	λ (μm)	$\Delta\lambda$ (μm)	F_ν (μJy)	Mag	Aperture radius ($''$)	References
R	0.70	0.22	1.1 ± 0.3	23.6	$1''.5 \times 3''.5^*$	McCarthy (1991)
J	1.25	0.38	15.0 ± 3.8	20.1	4.7	Iwamuro, private comm.
K'	2.13	0.34	43.7 ± 2.3	18.0	4.6	
N225.....	2.25	0.022	302 ± 7.4	–	4.6	
K -continuum core	2.13	0.32	12.6 ± 2.5	19.3	4.7	
K -continuum diffuse.....	2.13	0.32	15.0 ± 2.5	19.1	4.7	

* Flux density is extracted from the spectrophotometric data of $1''.5$ slit width and $3''.5$ spatial aperture.

Table 3. Emission-line properties of B3 0731+438.

Area	Size* ($'' \times ''$)	$F_\lambda(\text{continuum})^\dagger$ ($\text{W m}^{-2} \mu\text{m}^{-1}$)	$F(\text{line})^\ddagger$ (W m^{-2})	$W(\text{line})^\S$ (\AA)
Northern Cone.	3.596×1.740	$8.45(\pm 4.08) \times 10^{-19}$	$3.18(\pm 0.26) \times 10^{-19}$	1097_{-417}^{+1199}
Southern Cone.	1.856×2.204	$10.0(\pm 3.29) \times 10^{-19}$	$3.80(\pm 0.21) \times 10^{-19}$	1098_{-310}^{+645}
Central Core...	2.436×2.436	$1.47(\pm 0.03) \times 10^{-17}$	$1.74(\pm 0.03) \times 10^{-18}$	344 ± 14

* Size of the aperture used for photometry.

† Flux density of the continuum emission.

‡ Flux of the $\text{H}\alpha + [\text{N II}]$ emission lines.

§ Rest-frame equivalent width of the $\text{H}\alpha + [\text{N II}]$ emission lines.

Table 4. Physical properties in the emission-line cones of B3 0731+438 assuming a filling factor of 10^{-4} .

Area	V (cm^3)	n_e (cm^{-3})	M_{gas} (M_{\odot})	M_{tot} (M_{\odot})	Q (photons s^{-1})	Q_{tot} (photons s^{-1})	U
North	8.5×10^{68}	3.8×10	2.8×10^9	6.4×10^{10}	1.8×10^{55}	$> 6.1 \times 10^{56}$	$> 1.3 \times 10^{-3}$
South.	5.1×10^{68}	6.8×10	1.9×10^9	8.9×10^{10}	2.0×10^{55}	$> 1.4 \times 10^{57}$	$> 5.9 \times 10^{-3}$

Table 5. Simulated equivalent widths (in \AA) of $\text{H}\alpha + [\text{N II}]$ emission line by CLOUDY90.

		$n_{\text{H}} (\text{cm}^{-3})$		
		100	10	1
U	1	762	822	1054
	0.1	1229	973	952
	0.01	<u>1301</u>	<u>1300</u>	1119
	0.001	<u>1562</u>	<u>1561</u>	1561
	0.0001	1842	1842	1842

* Underlined are those of estimated physical parameters.

Table 6. Parameters for the best-fit models of the spectral energy distribution.

Model	A_V *	Age (Myr) [†]	Stellar Mass (M_{\odot}) [‡]
Instantaneous	1.9	500	3.4×10^{11}
Exponential ($\tau = 200$ Myr)	1.4	2000	6.5×10^{11}
Exponential ($\tau = 2$ Gyr)	1.4	10000	1.7×10^{12}

* Extinction of the type 2 AGN.

† Age of the galaxy.

‡ Stellar mass of the galaxy.

Figure 1. Color image of B3 0731+438, 11''8 on a side. The blue color is assigned to the line-subtracted K' -band image and the red color to the 2.25 μm narrow-band. Both images were smoothed by a 1 pixel Gaussian filter. Green is assigned to the average of the red and the blue image.

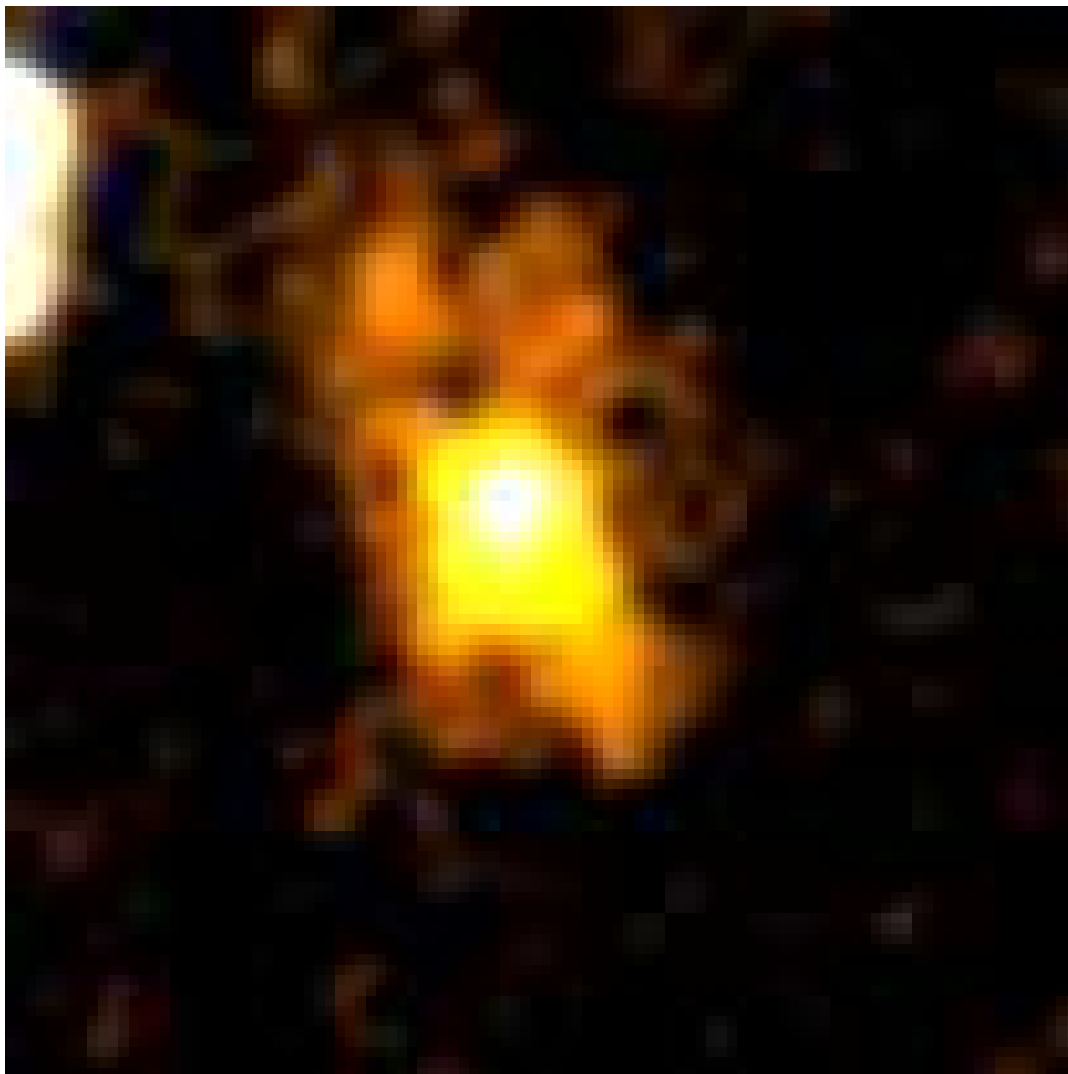


Figure 2. Logarithmic gray-scale images of B3 0731+438. The squares are the apertures with which aperture photometry was carried out, while the crosses indicate the position of 4710 MHz radio hot spots, as mapped by Carilli et al. (1997). (a) The $H\alpha$ + $[N\ II]$ image, smoothed by a Gaussian filter of 1 pixel. The first contour is at 1σ above the background level, while the subsequent contours are at levels of $2n\sigma$ ($n = 1, 2, 3, \dots$). σ is taken from the non-smoothed image. (b) The K -continuum image, which was smoothed by a 3 pixel Gaussian filter to match the seeing size with the $H\alpha$ + $[N\ II]$ image. The contours are at levels of $n\sigma$ ($n = 1, 2, 3, \dots$), where σ is again taken from the non-smoothed image. The profile at the lower-right corner is the contours of the stellar image used for deconvolution, whose peak value is normalized to B3 0731+438. (c) The K -continuum image deconvolved by MEM deconvolution method.

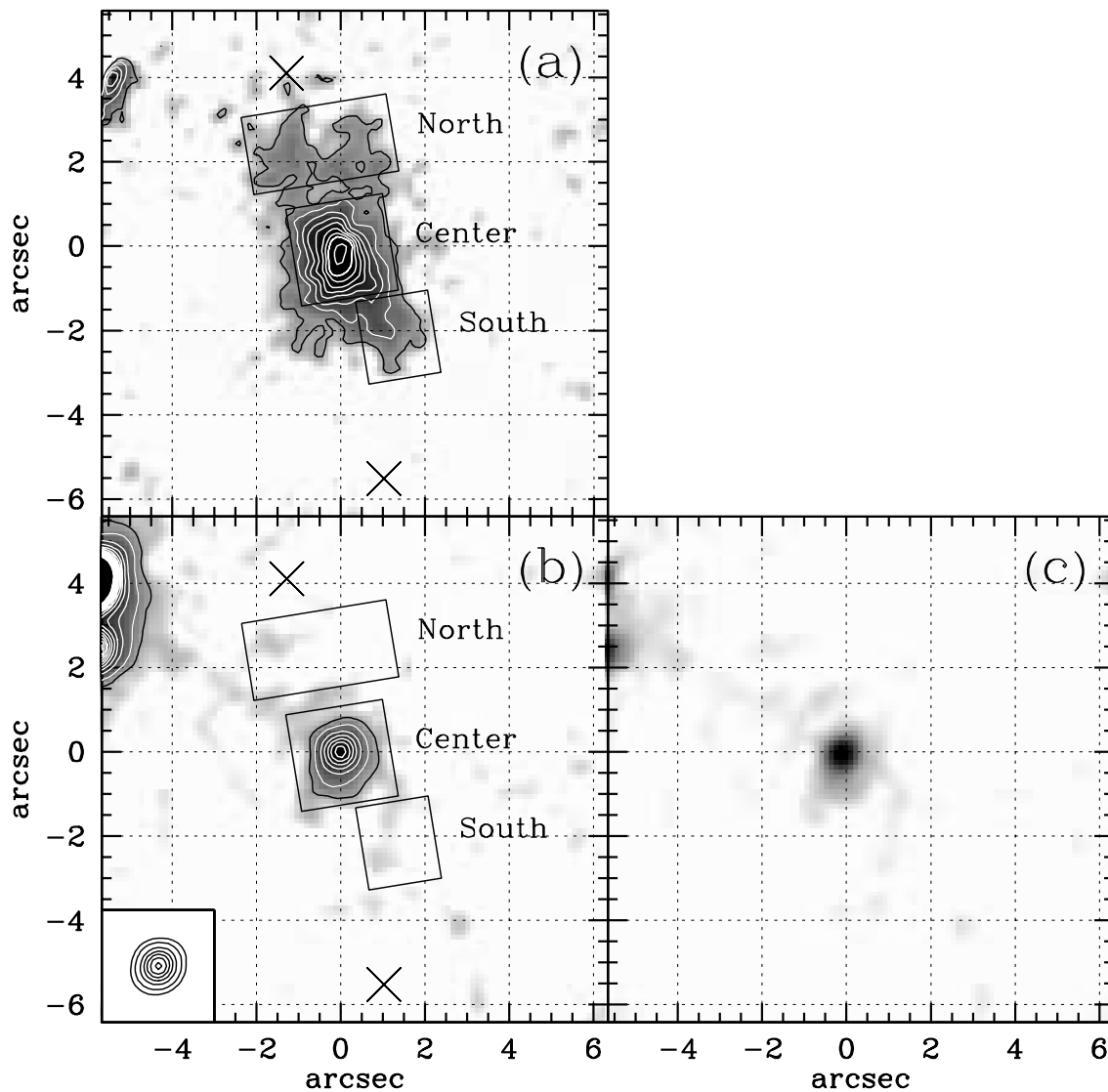


Figure 3. (upper-left) The K -continuum image of B3 0731+438. (upper-right) The best-fit two-component model profile of the K -continuum image. (lower-left) The stellar-profile subtracted K -continuum image, which reveals the underlying galaxy. (lower-right) The residual image after the two-component profile is subtracted.

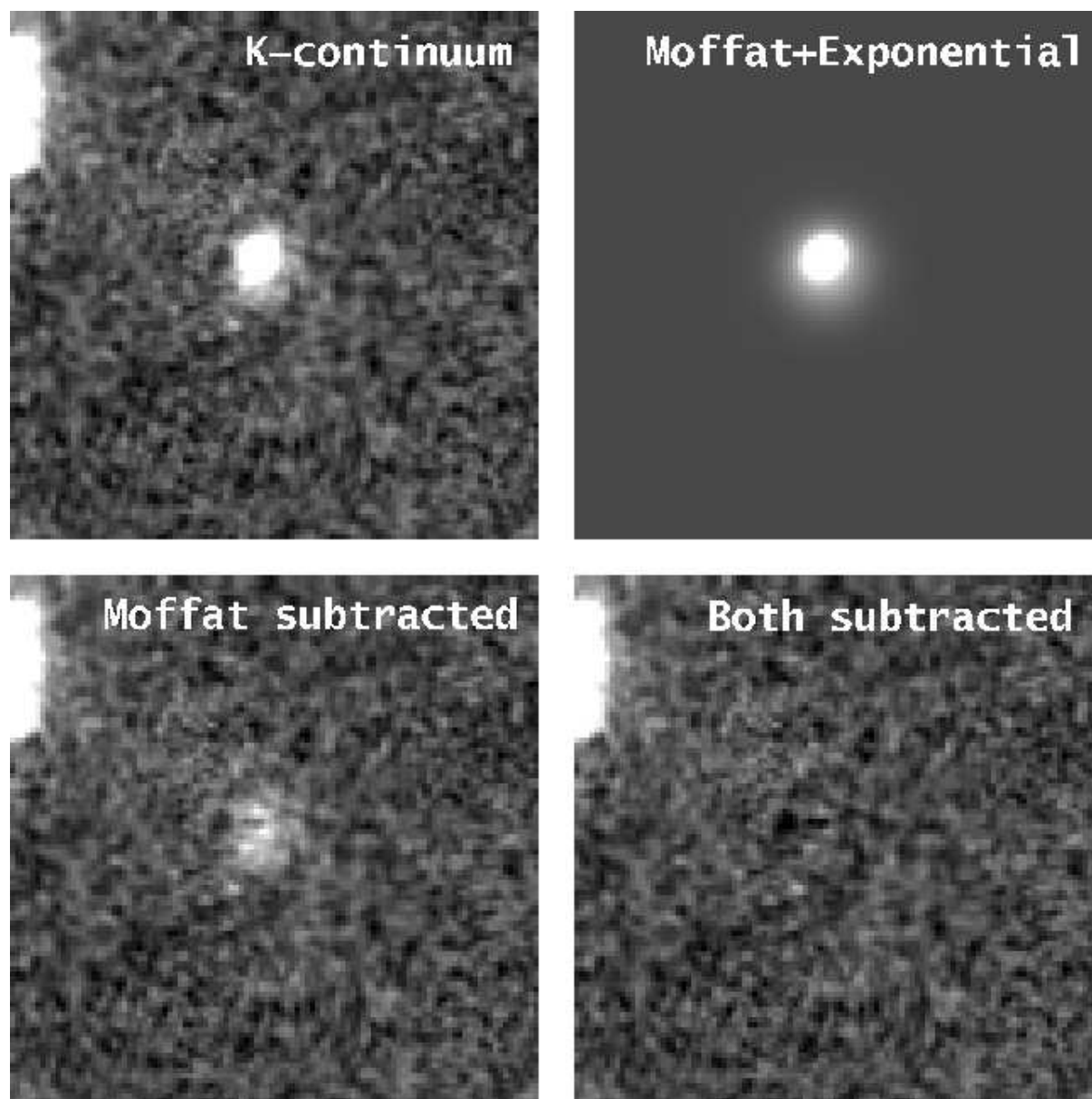


Figure 4. Spectral energy distribution of B3 0731+438. The open circle is from McCarthy (1991), the open square from Iwamuro (private communication), and the filled square from this work. The thick solid line is the best-fit models, and the thin solid line the spectra of (A) the type-2 AGN with dust extinction and (B) the galaxy-evolution model. The dotted line is the spectrum of the type-2 AGN without extinction. The star-formation models are: (a) instantaneous burst and (b) $\tau = 200$ Myr exponential burst.

